UC Berkeley

UC Berkeley Previously Published Works

Title

The influence of grain shape and volume fraction of sheet silicates on elastic properties of aggregates: Biotite platelets in an isotropic matrixElastic properties of aggregates

Permalink

https://escholarship.org/uc/item/1hb432xj

Journal

Geophysics, 79(6)

ISSN

0016-8033

Authors

Vasin, Roman
Lebensohn, Ricardo A
Matthies, Siegfried
et al.

Publication Date

2014-11-01

DOI

10.1190/geo2014-0148.1

Peer reviewed

eScholarship.org Powered by the California Digital Library
University of California

GEOPHYSICS, VOL. 79, NO. 6 (NOVEMBER-DECEMBER 2014); P. D433–D441, 6 FIGS., 2 TABLES.
10.1190/GEO2014-0148.1

The influence of grain shape and volume fraction of sheet silicates on elastic properties of aggregates: Biotite platelets in an isotropic matrix

Roman Vasin[1], Ricardo A. Lebensohn[2], Siegfried Matthies[3], Carlos N. Tomé[2], and Hans-Rudolf Wenk[4]

ABSTRACT

Elastic anisotropy of sheet-silicate-rich rocks such as shales and slates strongly depends on the orientation distribution of platelet-shaped minerals, as well as shape and orientation of pores. Bulk elastic anisotropy of the rock results in the anisotropy with respect to the propagation of elastic waves, and consequently, the fastest P-waves can travel with velocities exceeding the slowest velocities by a factor of two or even greater. An important factor is the sheet-silicate's grain shapes. We approached a model system of biotite platelets in an isotropic matrix with different methods: A mean-field self-consistent method that considered ellipsoidal particles in an effective anisotropic matrix, and a full-field method based on fast Fourier transforms that considered the microstructure, the topology of the polycrystal, and local interactions. Both methods provided numerically very close results. Using these results, we predicted that the aggregate with more oblate grain shape (thinner platelets) was elastically more anisotropic than the material with grains of less oblate shape, but only for small volume fractions of oriented platelets. For large fractions of platelets, the opposite was true. This switchover in the elastic anisotropy depended on texture strength, platelet shape, and elastic properties of the isotropic matrix.

INTRODUCTION

Sheet silicates with platelet-shaped grains are important components of many rocks such as gneisses and sedimentary shales. Their elastic properties are highly anisotropic (e.g., Aleksandrov and Ryzhova, 1961; Vaughan and Guggenheim, 1986; Militzer et al., 2011). Also, they are usually characterized by strong preferred crystallographic and morphologic orientations (e.g., Wenk et al., 2008, 2010, 2012). Thus, they contribute greatly to elastic anisotropy of rocks in the Earth's crust.

Commonly, bulk elastic properties of multiphase polycrystalline rocks are assessed with simple averaging models such as Voigt, Reuss, and Hill, which are not able to account for the effects of grain shapes in the elastic properties (e.g., Ivankina et al., 2005; Kern et al., 2008; Wang et al., 2009). These models perform averaging of single crystal elastic properties of different minerals over their crystal orientation distribution functions (ODFs) that relate the crystal orientations relative to sample coordinates. Also, it is commonly believed that oblate plate grain shape of sheet silicates and corresponding shape orientation distributions will lead to an increase in the calculated elastic anisotropy of rocks (e.g., Kern et al., 2008).

Consideration of grain shapes is possible within mean-field, self-consistent models, based on Eshelby's concept of ellipsoidal inclusions in a matrix (Eshelby, 1957). The shape orientations distributions (in the form of shape ODFs or SODFs) describe ellipsoidal particle shapes relative to sample coordinates. Recently, such a self-consistent method has been applied to calculate bulk elastic properties of biotite gneiss (Wenk et al., 2012) and shale (Vasin

Manuscript received by the Editor 31 March 2014; revised manuscript received 17 June 2014; published online 24 October 2014.
[1]University of California, Department of Earth and Planetary Science, California, USA and Joint Institute for Nuclear Research, Frank Laboratory of Neutron Physics, Dubna, Russia. E-mail: olddragon@mail.ru.
[2]Los Alamos National Laboratory, Materials Science and Technology Division, Los Alamos, USA. E-mail: lebenso@lanl.gov; tome@lanl.gov.
[3]University of California, Department of Earth and Planetary Science, California, USA and Muller Berset Str. 3, Dresden, Germany. E-mail: matthies.vinel@gmail.com.
[4]University of California, Department of Earth and Planetary Science, Berkeley, California, USA. E-mail: wenk@berkeley.edu.
© 2014 Society of Exploration Geophysicists. All rights reserved.

et al., 2013), based on their microstructural characteristics, including preferred orientations and grain shapes. Quite unexpectedly, it has been found that anisotropic grain shape of sheet silicates increases elastic anisotropy of rocks containing small amounts of platelet-shaped grains (gneiss with ~20% of biotite) and reduces elastic anisotropy of rocks with large amounts of platelet-shaped grains (shale with ~70% of sheet silicates). Also, in both cases, model rocks with assumed spherical grain shapes of sheet silicates are characterized by higher values of quasilongitudinal elastic wave velocities than rocks with platelet-shaped sheet silicate grains (Table 1). Was this simply an artifact of the mean-field approximation used, or some kind of intrinsic limit? In this contribution, we perform calculations on a simple model system of biotite within an isotropic matrix, using different averaging approaches. Comparing mean-field methods with ellipsoidal inclusions with full-field simulations that consider the local micromechanical fields, we obtain similar results and confirm that the grain-shape/volume-fraction effect is a real physical characteristic.

MODELING AND AVERAGING METHODS

Calculation of bulk elastic properties and elastic wave velocities in polycrystals

We review here the case of a two-phase model rock consisting of biotite grains in an isotropic matrix. We are interested in linear elastic properties of this model material that are described with the twice-symmetric, fourth-rank stiffness tensor C_{ijkl} (or compliance tensor $S_{ijkl} \equiv C^{-1}_{ijkl}$) that we will represent in standard two-index Voigt notation.

Voigt (1887) and Reuss (1929) models are often used to calculate bulk elastic properties of polycrystals, based on single crystal elastic properties and ODFs. They are based on different physical assumptions (crystallites are subjected to the same strain or same stress, respectively) and determine maximum and minimum bounds for elastic properties of a polycrystal. Their results can be fairly different if single crystals with high elastic anisotropy and/or multiphase aggregates with high contrast in elastic properties are considered. These averages are not able to take grain shapes into account. Consideration of grain shapes (approximated by ellipsoids) is possible within a self-consistent scheme (e.g., Kröner, 1958; Morris, 1970; Kocks et al. [2000], Chapter 7) based on Eshelby's (1957) concept of ellipsoidal inclusions in a homogeneous matrix. Here, we use two slightly different variants of the self-consistent approach.

The first is GeoMIXself (GMS) (Matthies, 2010). A characteristic feature of this algorithm is that on each self-consistent iterative step, two effective elastic tensors are calculated for the whole material, one based on stiffness and the other based on compliance averaging, and a "symmetric square root" operation (Matthies, 2012) is applied to get a single solution for bulk elastic properties (i.e., stiffness is the inverse compliance). Currently, it is possible to enter up to four phases, three of which can have associated grain shapes and orientation distributions, and the fourth one is a "matrix." Textures of different phases have to be entered in the form of discrete distribution functions with $5° \times 5° \times 5°$ resolution, resulting in the most general case in approximately 200,000 unique orientations with corresponding orientation densities for each phase. Despite 5° resolution of input ODFs, Eshelby tensors are calculated with 1° steps to ensure good precision of the results in case of extremely anisotropic constituents of the polycrystal, such as graphite grains (Matthies, 2012).

The second one is the elastic self-consistent (ELSC) module implemented in the viscoplastic self-consistent (VPSC) code (Lebensohn and Tomé, 1993). The self-consistent approaches are based on treating each grain as an ellipsoidal inclusion embedded in and interacting with an effective medium having the overall properties of the aggregate. With ELSC, we find the (unknown) elastic properties of aggregates using the (known) elastic properties of the constituent grains. Ellipsoids with different shapes and orientation can be assigned to each grain, and grains can have different anisotropic elastic properties if they belong to a multiphase aggregate. Here, the input ODF is in the form of a set of individual orientations. This method also guarantees that resulting aggregate stiffness and compliance are the inverse of each other.

Finally, we apply a full-field method based on the fast Fourier transform (FFT), a method originally developed by Moulinec and Suquet (1998) to compute the local and effective mechanical response directly from an image of a composite material in which the source of heterogeneity is related to the spatial distribution of phases with different mechanical properties. The FFT-based approach has been adapted by Lebensohn (2001) to deal with single-phase or multiphase polycrystals (in which the heterogeneity is related to the spatial distribution of crystals with directional mechanical response), deforming in different regimes, elastic (Brenner et al., 2009), viscoplastic (Lebensohn et al., 2008), or elastoviscoplastic

Table 1. Minimum $V_{P\,min}$ and maximum $V_{P\,max}$ quasilongitudinal elastic wave velocities, coefficient of elastic anisotropy $k_P = 200 * (V_{P\,max} - V_{P\,min})/(V_{P\,max} + V_{P\,min})$, and maximum S-wave splitting $\Delta V_{S\,max}$ in some model sheet-silicates-bearing rocks (without pores and cracks).

	Model biotite gneiss (no pores), based on (Wenk et al. [2012], Table 3) and density of 2.75 g/cm^3		Model shale (no pores), based on (Vasin et al. [2013], Table 5) and density of 2.648 g/cm^3		
Grain shape of sheet silicates	Sphere {1:1:1}	Platelet {1:0.2:0.05}	Sphere {1:1:1}	Platelet {1:1:0.1}	Platelet {1:1:0.05}
$V_{P\,min}$, m/s	5551	5464	5535	5311	5285
$V_{P\,max}$, m/s	6235	6235	6366	6067	6017
k_P, %	11.6	13.2	14.0	13.3	12.9
$\Delta V_{S\,max}$, m/s	472	530	379	338	327

(Lebensohn et al., 2012). The formulation is conceived for periodic unit cells and provides an exact solution of the governing equations of equilibrium and compatibility. The elastic version of the method is based on the fact that the local response of a heterogeneous medium can be calculated as a convolution integral between the Green function associated with the displacement field of the reference homogeneous medium and a polarization field, which is a function of the sought solution. Fourier transforms can reduce convolution integrals in real space to simple products in Fourier space, and the efficient FFT algorithm can be used to obtain the strain fields by transforming back into Cartesian space. However, because the polarization field depends on the a priori unknown micromechanical fields, an iterative scheme has to be implemented to obtain, upon convergence, a compatible strain and stress fields in equilibrium.

The application of these methods requires the knowledge of single-crystal elastic constants of all constituent phases, their volume fractions, orientation distributions (SODF, shape or morphologic texture, and ODF) and grain shapes. In the FFT-based full-field case, the exact topology of the multiphase polycrystal, described in terms of a regular grid of Fourier points (FPs) belonging to either the isotropic matrix or a given single-crystal biotite grain, is also required.

All methods provide an elastic tensor of the material. From it, elastic wave velocities can be calculated using Christoffel equations and bulk material density in a so-called long-wave approximation (wavelength $\gg$ size of heterogeneities in the material). Because Christoffel equations require the knowledge of the propagation direction, we calculated phase velocities of elastic waves in different directions of our model rock using a $5° \times 5°$-grid. Often of practical interest are values of the P-wave anisotropy coefficient $k_p(\%) = 200 * (V_{\mathrm{P\,max}} - V_{\mathrm{P\,min}})/(V_{\mathrm{P\,max}} + V_{\mathrm{P\,min}})$ and maximum S-wave splitting $\Delta V_{\mathrm{S\,max}} = (V_{\mathrm{S1}} - V_{\mathrm{S2}})|_{\max}$ that can be easily calculated from known elastic wave velocities patterns.

Elastic properties and density of minerals in the model

Most sheet silicates are monoclinic. But for biotite, we are using single-crystal elastic properties that have been measured by Aleksandrov and Ryzhova (1961), assuming hexagonal symmetry with $C_{11} = C_{22} = 186.0$, $C_{33} = 54.0$, $C_{13} = C_{23} = 11.6$, $C_{44} = C_{55} = 5.8$, $C_{66} = 76.8$, $C_{12} = C_{11} - 2C_{66} = 32.4$ (GPa), and all other components are equal to zero. The Young's modulus of a hexagonal biotite single crystal is shown in Figure 1. It is stiffest for directions in the sheet plane $X_B Y_B$ but not softest in the Z_B-direction. We also assume hexagonal crystal symmetry for defining the ODF.

To specifically highlight the influence of biotite grain shapes, ODFs, and volume fraction on bulk elastic properties of the whole model rock, results will be presented for an isotropic matrix with Young's modulus $E = 40$ GPa and Poisson's ratio $\nu = 0.3$. Cases of harder matrix ($E = 80$ GPa) behavior are also considered and illustrated for elastic wave velocities. Within the ELSC scheme, matrix isotropy is enforced by considering 500 randomly oriented FCC grains with isotropic elastic constants.

To calculate elastic wave velocities from a stiffness tensor, a bulk density value is required. We use a density of 3.05 g/cm^3 for biotite and isotropic matrix to simplify the interpretation of elastic wave velocities dependencies on biotite content in the model.

Coordinate systems and orientation distributions

In general, three different coordinate systems (Cartesian, right-handed) are required to describe orientation relationships in a polycrystalline material with nonspherical grain shapes. Bulk elastic properties of whole material are given with respect to a macroscopic sample coordinate system $K_A\{X_A, Y_A, Z_A\}$ (Figure 2a). Physical properties of single crystals are usually given in a crystal coordinate system $K_B\{X_B, Y_B, Z_B\}$, that is related to the unit cell according to a set of specific rules (e.g., Nye, 1957; Matthies et al., 1987, 1988) (Figure 2b). The ODF is a probability density for a volume element of polycrystalline material to have a certain orientation K_B with respect to K_A. A grain coordinate system $K_E\{X_E, Y_E, Z_E\}$ is related to the shape of the ellipsoidal grain, and its axes are set parallel to the axes of an ellipsoid (Figure 2c), and the orientation relation of K_E with respect to K_B needs to be defined.

There are two extreme cases for defining K_E. In our case with "hexagonal" biotite, K_E is directly related to the crystal axes, such that $K_B = K_E$ (i.e., the crystal c axis Z_B is parallel to the shape Z_E axis, and we have [001] platelets). In the case of crystals in a metal with a rolling texture, the grains are flat ellipsoids directly related to sample axes ($K_A = K_E$) and independent of crystal orientation.

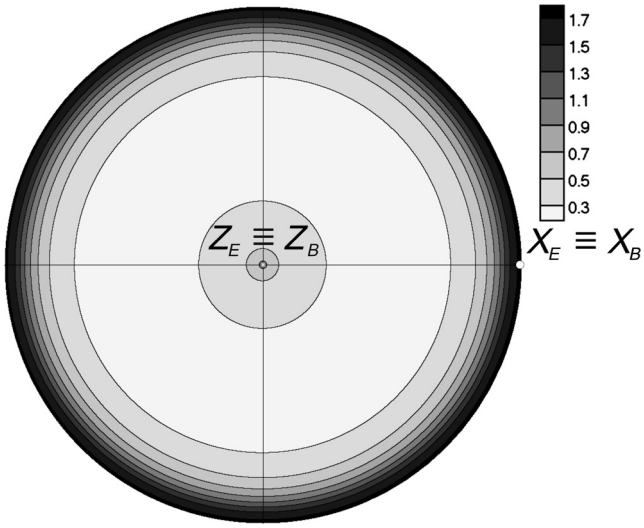

Figure 1. Young's modulus of biotite single crystal (units of 100 GPa), equal area projection, linear scale. The minimum value is 20.5 GPa, and the maximum value is 178.6 GPa.

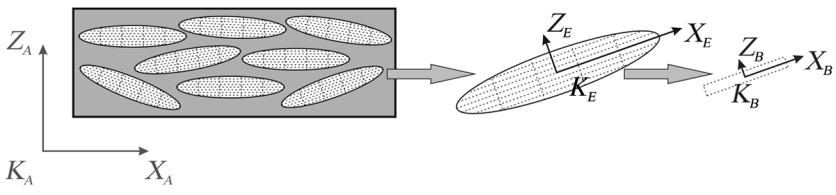

Figure 2. Definition of coordinate systems. (a) Sample coordinate system K_A with ellipsoidal grains, (b) crystal coordinate system K_B, and (c) grain coordinate system K_E.

Sheet silicates belong to the first case. They display a characteristic morphology with grains of thin oblate ellipsoidal, or platelet-like, shape parallel to monoclinic (001) crystal planes, or (100) if the first monoclinic setting is used for the crystal. Thus, inside each biotite platelet, a crystal lattice, and its associated K_B, is fixed with a certain orientation relationship to K_E (Figure 2b and 2c). In sheet silicates possessing monoclinic or triclinic lattices, K_E is tilted with respect to K_B (e.g., in triclinic crystals, the direction normal to the [001] plane is not parallel to [001] direction). Thus, in such cases, additional rotations have to be performed to consider the difference between K_E and K_B (Vasin et al., 2013). In our simplified case of hexagonal biotite, K_B is parallel to K_E. As a consequence, ODF ≡ SODF and the shortest grain dimension is parallel to $Z_E \equiv Z_B || [001]$. Care should be taken when deriving the SODF from the ODF. The ODF assumes crystal symmetry, whereas the SODF satisfies orthorhombic particle shape symmetry.

There are some differences among the GMS, ELSC, and FFT. In GMS and ELSC, all grains have the same ellipsoidal shape that is linked to the crystal system, but they have a different ellipsoid orientation (Figure 3a and 3b). In GMS, it is assumed that ODF and SODF are linked in a systematic statistical way and the transformation $K_B \rightarrow K_E$ applies to the whole distribution. In ELSC, the relationship is defined for each individual grain. In FFT, grain shapes vary. They are obtained by first creating a random grain distribution (Figure 3c) and then deforming this microstructure to the desired aspect ratio (Figure 3d). Thus, effective grain shapes are related to the sample coordinate system K_A. This introduces some discrepancy between the mean-field and the full-field predictions, but we expect it to be minor in the present case of a strong preferred orientation.

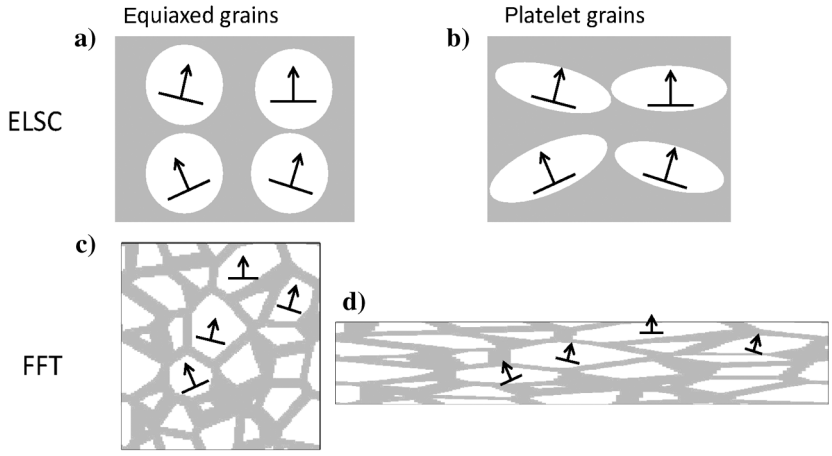

Figure 3. Schematic representation of the microstructure for (a and b) ELSC and (c and d) FFT. In ELSC, all grains have the same ellipsoidal shape, and in panel (b), each ellipsoid's orientation is linked to the crystal (arrows). The ellipsoids are not spatially correlated. In FFT, the original microstructure (c) is randomly generated and equiaxed and changed into platelets (d) by stretching the sample. In panels (b and d), the ellipsoids and the unit cell, respectively, are not to scale for the cases $\zeta = 0.1$ and 0.01 considered here.

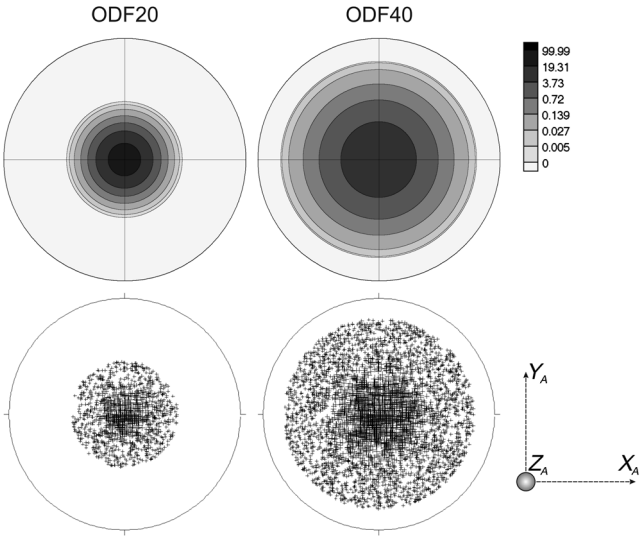

Figure 4. Pole figures (001) of biotite, for ODF 20 and ODF 40, based on discrete $5° \times 5° \times 5°$ ODFs (above) and individual orientations (below). Equal area projections. Pole densities in multiples of a random distribution, log scale for contours; for individual orientations, large symbols mean larger weight.

Sheet silicates in real rocks often have preferred orientation patterns that are close to axisymmetric (or fiber) textures, and the axis of the fiber is perpendicular to the macroscopic bedding or foliation plane of the rock (e.g., Wenk et al., 2010). For simplicity, we use a perfect fiber texture for biotite grains, with a fiber axis parallel to Z_A and perpendicular to the foliation plane $X_A Y_A$. Elastic properties of materials with fiber texture can be described with only five independent C_{ij}'s, $C_{11} = C_{22}$, C_{12}, $C_{13} = C_{23}$, C_{33}, $C_{44} = C_{55}$, and $C_{66} = (C_{11} - C_{12})/2$ with all others being zero.

Following this, we construct two ODFs using standard Gaussian fiber components (Matthies et al., 1987) of different full-width at half-maximum (FWHM):

- ODF 20: FWHM = 20°, texture index $F_2 = 22.82$
- ODF 40: FWHM = 40°, texture index $F_2 = 5.75$,

to investigate the influence of the texture strength on bulk elastic properties of our model two-phase rock. Corresponding pole figures of shortest grain dimensions (001) (or $Z_B = Z_E$) are shown in Figure 4. For use in GMS routines, these ODFs are represented in a discrete $5° \times 5° \times 5°$ grid in the orientation space. For the ELSC and FFT calculations, 5000 randomly selected individual orientations were assigned corresponding ODF values. Only those with nonzero ODF values have been further considered for calculations (e.g., for ODF 20, only 1038 out of 5000 individual orientations had nonzero ODF values).

Biotite grain shapes

The applied methods for calculation of bulk elastic properties of polycrystals are size independent and only ratios of grain axes are to be taken into account. Thus, in K_E, biotite particle axes can be defined as $\{1:1:\zeta\}$. For spherical grains $\zeta = 1$, and for platelet-shaped grains $\zeta < 1$. In real rocks a distribution of grain shapes of sheet silicates is usually observed, with ζ roughly in the interval

between 0.01 and 0.1 (e.g., Vasin et al., 2013). In our simple model, we consider biotite grain shapes with $\zeta = 0.1$ and 0.01 and compare them with the case of spherical grains.

RESULTS

For each given biotite ODF, SODF, and grain shape, we calculate elastic properties of our model rock with mean-field self-consistent methods, for different biotite content from 0% to 100%, in 5% increments.

Additionally, to provide reference solutions for validation of the above mean-field estimations, the full-field FFT-based model was used to calculate the local fields and effective elastic properties for the ODF 20 crystallographic texture, different biotite grain shapes ($\zeta = 1$, 0.1, and 0.01), and biotite volume fractions of: 0% (no biotite, only isotropic matrix material), 31.1%, 48.6%, 71.4%, 84.4%, and 100% (no matrix, single-phase biotite polycrystal). The microstructures corresponding to these cases were built as follows:

1) A periodic Voronoi tessellation with 100 domains, discretized by a $128 \times 128 \times 128$ Fourier grid, was initially generated.
2) The 100 orientations from ODF 20 with the largest volume fractions were randomly assigned to each domain (the 100% biotite case).
3) All FPs with at least one first, second, and third nearest neighbor belonging to a different grain were identified, removed from the corresponding grain, and assigned to the isotropic matrix, resulting in 71.4%, 48.6% (see Figure 3c), and 31.1% volume fraction of biotite, respectively. In the case of the first nearest neighbor, choosing only one FP from each pair, the aggregate with highest biotite content in the matrix (84.4%) was obtained;
4) To obtain unit cells with equiaxed ($\zeta = 1$) and platelet-shaped grains ($\zeta = 0.1$ and 0.01), the following distances between FPs in X_A, Y_A, and Z_A directions were adopted: (1:1:1), (2.15:2.15:0.215), and (4.64:4.64:0.0464), respectively. Figure 3d shows a 2D section of the unit cell corresponding to platelet grains (not to scale).

All of the methods (mean-field and full-field) give qualitatively and quantitatively very similar results for C_{ij}, as is shown in Table 2 for the case ODF 20 and isotropic matrix with $E = 40$ GPa and $\nu = 0.3$, for 48.6% biotite content and two different grain shapes. More generally, the results are shown in Figure 5 for the same ODF, matrix, and different biotite grain shapes and volume fractions. Note that, for the sake of clarity, the curves corresponding to the different models are shifted with respect to each other; otherwise, they would be almost coincident. This figure shows a crossing of the equiaxed and platelet curves at approximately 75%–85% biotite for C_{11} and C_{66}, and at approximately 40%–50% biotite for C_{13} and C_{44}, whereas the C_{12} and C_{33} curves do not cross.

More specifically, elastic constants calculated with GMS and ELSC differ by less than 2GPa. The small differences are mostly due to the relatively low number of individual orientations used to describe orientation distribution of biotite grains in the VPSC code; e.g., in the ODF 20 case, there are 1038 nonzero ODF values, that is, approximately 35 times lower than the number of $5° \times 5° \times 5°$ cells in orientation space with nonzero ODF values used by GMS. On the other hand, calculation times for ELSC are approximately two orders of magnitude less than for GMS. The precision of ELSC could be improved by using a larger number of orientations.

Because all methods yield similar elastic constants, we will only show elastic wave velocities and anisotropy coefficients calculated from elastic properties obtained with GMS. Figure 6 shows P-wave anisotropy k_p and maximum S-wave splitting $\Delta V_{S\,max}$ for different models. Results for Voigt and Reuss methods are plotted for comparison.

It should be noted that $V_{P\,max}$ is always associated with a vector in the $X_A Y_A$ plane (90° to the fiber texture axis). However, $V_{P\,min}$ is not necessarily associated with a vector parallel to Z_A. In fact, this direction is inclined to Z_A by an angle in the 0°–35° interval. This angle's value depends on texture strength, shape of biotite grains, and biotite content. It happens because the minimum Young's modulus of biotite is not in the $Z_B = Z_E$ direction, but in a direction inclined to it (Figure 1). The consequence is that, as we made velocities calculations in different directions of the model rock every 5°, our $V_{P\,min}$ value can be overestimated. The overall change of $V_{P\,min}$ with the change of biotite content is relatively small (especially compared to changes of $V_{P\,max}$). This small error should not have a profound influence on the results and k-values.

Table 2. Comparison of the three different methods for the calculation of effective elastic properties. Elastic constants (in K_A) of model two-phase rock consisting of 48.6% of biotite grains with $\zeta = 1$ and 0.01 and ODF 20 and isotropic matrix with $E = 40$ GPa and $\nu = 0.3$. All values are in gigapascal. All other values are close or exactly equal to zero.

Aspect ratio	$\zeta = 1$			$\zeta = 0.01$		
Model	GMS	ELSC	FFT	GMS	ELSC	FFT
C_{11}	87.7	87.3	87.6	97.2	96.8	102.0
C_{12}	27.2	27.2	27.2	26.4	26.4	25.4
C_{13}	21.5	21.6	20.7	21.8	22.0	20.7
C_{22}	87.7	87.5	87.6	97.2	97.2	102.0
C_{23}	21.5	21.5	20.7	21.8	21.9	20.7
C_{33}	52.4	52.3	53.0	51.9	51.8	52.5
C_{44}	11.1	11.2	10.4	11.0	11.1	10.4
C_{55}	11.1	11.2	10.4	11.0	11.1	10.4
C_{66}	30.2	30.1	30.6	35.4	35.3	38.8

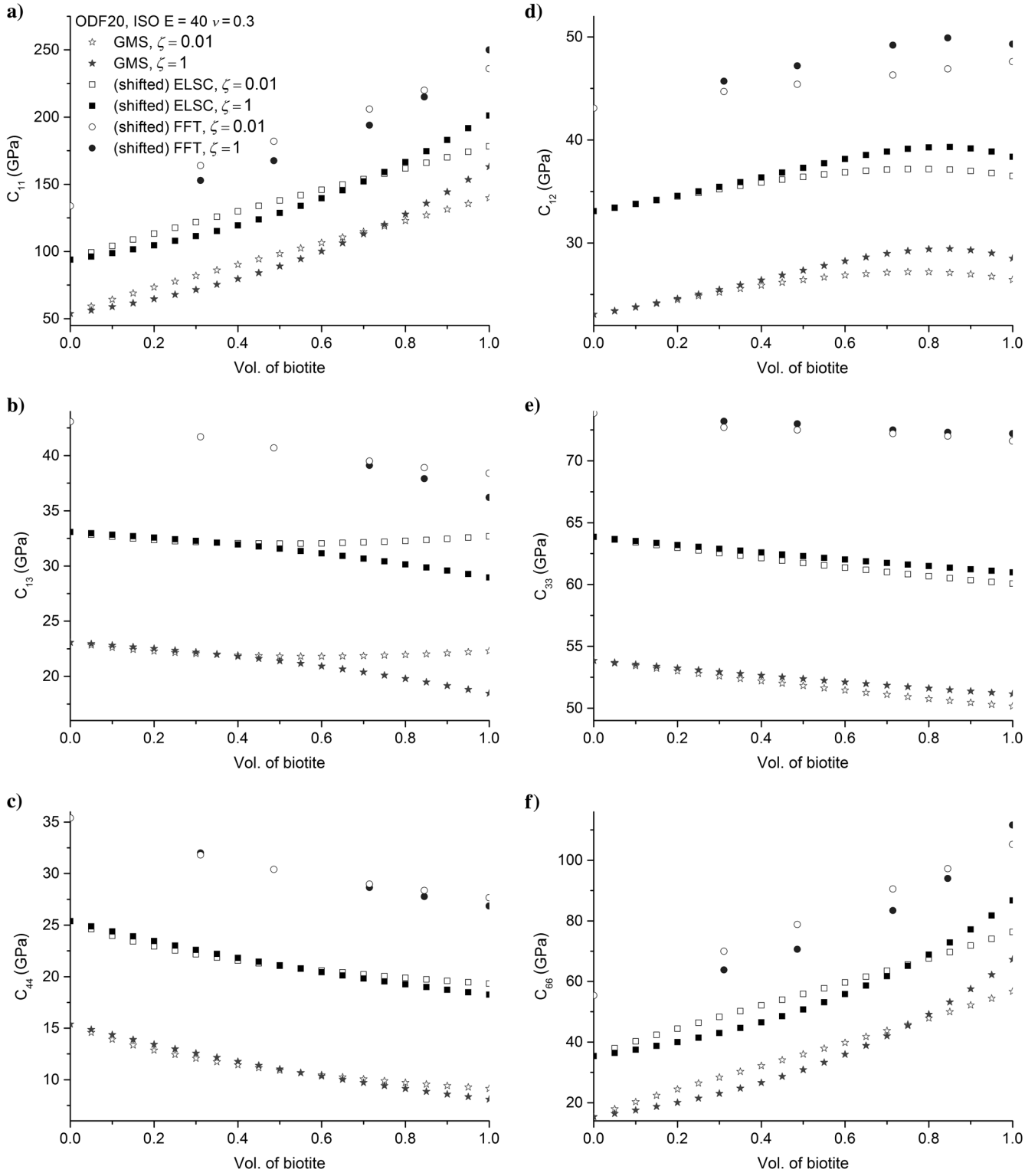

Figure 5. Comparison of C_{ij}'s as function of biotite content for the three different methods for the calculation of effective elastic properties: GMS, EPSC, and FFT. Biotite with ODF 20 texture and grain aspect ratios $\zeta = 1$ and 0.01 in an isotropic matrix with $E = 40$ GPa and $\nu = 0.3$. GPa units apply to GMS. Other curves are shifted 40 GPa for ELSC and 80 GPa for FFT for C_{11}, and 10 GPa for ELSC and 20 GPa for FFT for C_{12}, C_{33}, C_{13}, and C_{44}, and 20 GPa for ELSC and 40 GPa for FFT for C_{66}.

Also, $V_{P\,min}$ and $V_{P\,max}$ are not only minimum and maximum phase velocities, but also minimum and maximum group velocities (e.g., Dewhurst and Siggins, 2006). The same is true for $\Delta V_{S\,max}$-values that are the same, independently if phase or group velocities are used for the calculation. Minimum S-wave splitting, as for all materials possessing axial symmetry, is equal to zero for our model rocks.

Figure 5 shows that for a biotite fraction of 1.0, a model rock with spherical biotite grains has higher C_{11} and C_{66}, but lower C_{44} than that with biotite platelets. This results in higher k_p and $\Delta V_{S\,max}$ for a model rock composed of 100% biotite spherical grains (e.g., Figure 6a and 6d). By contrast, a rock with high content of biotite platelets is less anisotropic with regard to elastic wave propagation.

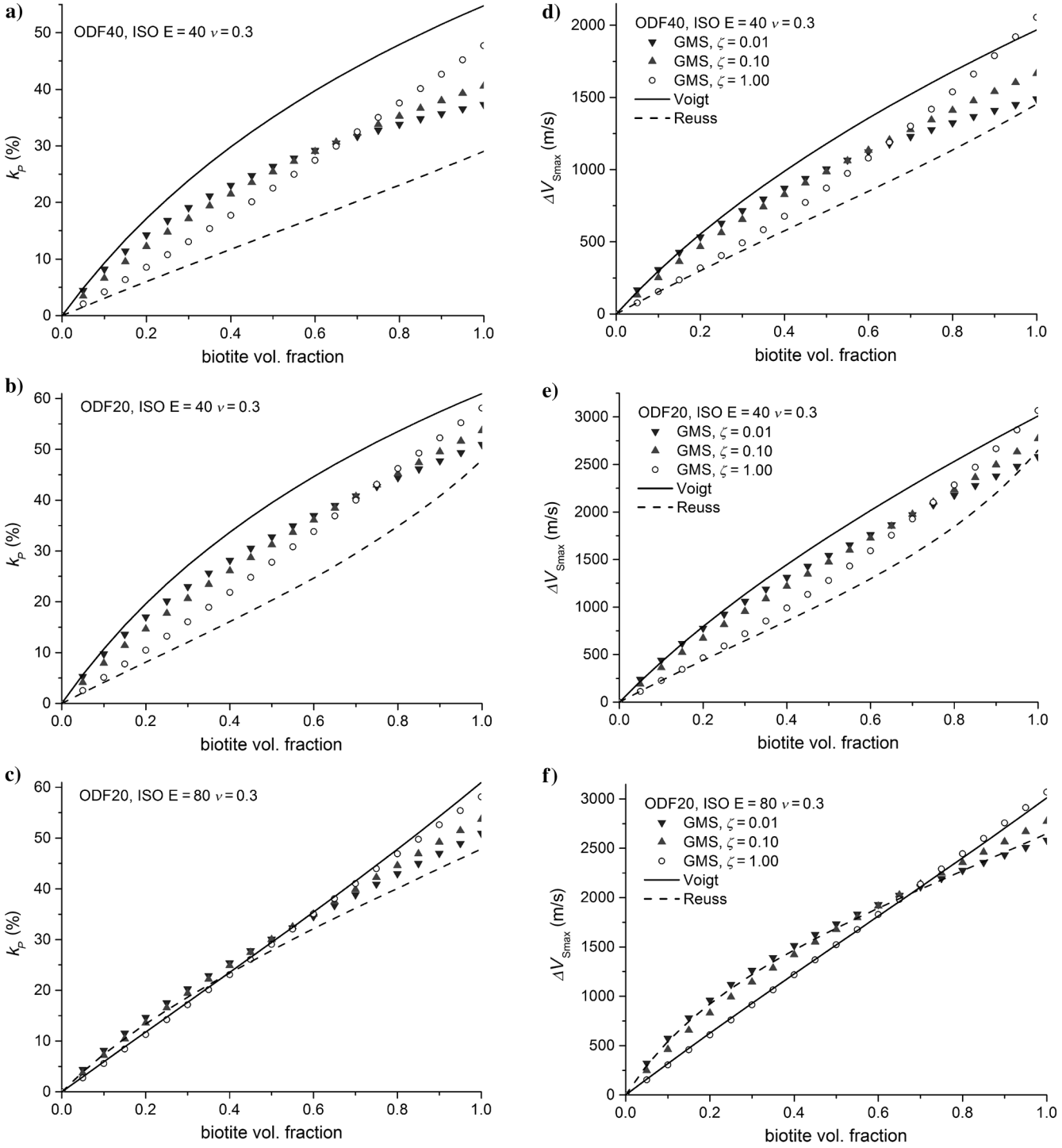

Figure 6. (a-c) P-wave velocity anisotropy coefficient k_P and (d-f) maximum S-wave splitting $\Delta V_{S\,max}$ as function of biotite fraction for GMS model ($\zeta = 1, 0.1$ and 0.01, $\nu = 0.3$); Voigt and Reuss averages are shown for comparison. (a and d) ODF 40, isotropic matrix with $E = 40$ GPa, (b and e) ODF 20, $E = 40$ GPa, and (c and f) ODF 20, $E = 80$ GPa.

However, at a low biotite content, the situation is reversed. An aggregate with low content of biotite platelets has higher C_{11} and C_{66}, and lower C_{44} than an aggregate with the spherical biotite grains.

Dependencies of C_{11}, C_{44}, and C_{66} with biotite content (for all considered combinations of biotite ODFs and matrix properties) and, consequently, the k_P (Figure 6a and 6c) and $\Delta V_{S\ max}$ (Figure 6d and 6f) dependencies show certain "critical" biotite contents at which the corresponding curves for spherical and platelet biotite grains cross each other. At this critical biotite content, certain elastic characteristics of the two-phase composite are independent on the platelet shape. In case of the weaker ODF 40, a critical biotite content also appears on C_{33} curves (not shown). In aggregates with sharper biotite texture (ODF 20), for the case of spherical biotite grains, a higher C_{33} value was obtained than for biotite platelets, but only by 1–2 GPa.

Dependencies of k_P and $\Delta V_{S\ max}$ on biotite content for some combinations of matrix properties and biotite texture strength are shown in Figure 6. The critical biotite contents for these dependencies shift toward lower biotite content with decrease in texture strength. Values of these critical biotite contents for k_P strongly depend on the Young's modulus of the isotropic matrix. The stiffer the matrix, the less biotite content is needed for material with spherical biotite grains to become more elastically anisotropic than material with biotite platelets (see Figure 6c and 6f).

DISCUSSION

All the models provide numerically similar results. It is reassuring to observe the same predicted behavior with mean-field approaches and the full-field FFT-based method, considering that the latter accounts for heterogeneity and spatial grain correlations.

At a higher biotite content, all model rocks consisting of an isotropic matrix aggregate with spherical biotite grains are more anisotropic with respect to elastic wave propagation: k_P and $\Delta V_{S\ max}$ are always higher for material with spherical grains. Thus, the effect of reduction in elastic wave propagation anisotropy when platelet-shaped biotite grains (instead of spherical grains) are considered is not an artifact of the averaging method.

Critical points appear on C_{ij} dependencies on biotite content for some combinations of isotropic matrix properties and biotite texture strength (Figure 5). This is particularly clear for C_{11} and C_{66}. Critical points for FFT are somewhat shifted relative to GMS and ELSC, and we attribute it to the different definitions of the particle shape coordinate system as discussed earlier. In FFT, the shape is linked to the sample, and in GMS and ELSC, it is linked to the crystal. Similar points exist for velocity dependencies such as P-wave anisotropy k_P and S-wave splitting $\Delta V_{S\ max}$ (only shown for GMS in Figure 6), though the critical biotite content for different dependencies may be different. If the biotite content in a model rock is higher than the critical content, the k_P coefficient of the rock with biotite platelets becomes closer to that of Reuss model, whereas the k_P of the rock with spherical biotite grains is closer to that of Voigt model, and the reverse is true for low biotite content. We note, that, for example, k_P of the model two-phase rock with a certain critical biotite content is largely independent of the biotite platelet aspect ratio ζ.

At low biotite content, all model rocks with platelet-shaped biotite grains are more anisotropic with respect to elastic wave propagation. The transition depends on the elastic coefficients of the biotite and the matrix, as well as texture strength. The biotite content at the k_P critical point decreases with the increase in the Young's modulus of the isotropic matrix and with the decrease in the biotite texture strength.

CONCLUSION

Using different modeling techniques, we document the effect of particle shape on elastic properties in a two-phase composite with platelets. Interestingly, there is a consistent crossover, relative to spherical particles, which depends on particle content and also on elastic properties of particles and matrix. It would be interesting to see if such effects can also be observed experimentally, for example, P-wave anisotropy in silt-clay mixtures.

ACKNOWLEDGMENTS

The authors would like to acknowledge support from National Science Foundation (NSF) (EAR-1343908) and Department of Energy (DOE) (DE-FG02-05ER15637). We are appreciative for comments from the editor and three reviewers that helped improve the manuscript.

SUMMARY OF ACRONYMS AND SYMBOLS

ODF	=	Orientation distribution function, a mathematical description of preferred orientation of crystals relative to sample coordinates
SODF	=	Shape orientation distribution function, preferred orientation of morphologic features (e.g., nonequiaxed ellipsoidal grains) relative to sample coordinates
ELSC	=	Elastic self-consistent (mean-field averaging method)
GMS	=	GeoMIXself (mean-field averaging method), which combines geometric mean and the standard ELSC
FFT	=	Fast Fourier transform (full-field averaging method)
FP	=	Fourier point, point of the discrete grid used to model the material with the FFT method
K_A	=	a coordinate system related to the sample
K_B	=	a coordinate system related to the crystal lattice
K_E	=	a coordinate system related to the grain morphology (represented by an ellipsoid)
C_{ij}	=	elastic tensor of the material (stiffness)
S_{ij}	=	elastic tensor of the material (compliance)
E	=	Young's modulus
ν	=	Poisson's ratio
ζ	=	aspect ratio of platelet-shaped grains
k_P	=	P-wave anisotropy coefficient that demonstrates the anisotropy of the material with respect to (quasi) P-wave propagation
$\Delta V_{S\ max}$	=	maximum S-wave splitting, i.e., the maximum difference between velocities of primary and secondary (quasi) S-waves

REFERENCES

Aleksandrov, K. S., and T. V. Ryzhova, 1961, The elastic properties of rock-forming minerals. Part: II: Layered silicates: Izvestiya, Academy of Sciences USSR, Geophysics Series, **12**, 1799–1804.

Brenner, R., R. A. Lebensohn, and O. Castelnau, 2009, Elastic anisotropy and yield surface estimates of polycrystals: International Journal of Solids and Structures, **46**, 3018–3026, doi: 10.1016/j.ijsolstr.2009.04.001.

Dewhurst, D. N., and A. F. Siggins, 2006, Impact of fabric microcracks and stress field on shale anisotropy: Geophysical Journal International, **165**, 135–148, doi: 10.1111/j.1365-246X.2006.02834.x.

Eshelby, J. D., 1957, The determination of the elastic field of an ellipsoidal inclusion, and related problems: Proceedings of the Royal Society of London, Series A, **241**, 376–396, doi: 10.1098/rspa.1957.0133.

Ivankina, T. I., H. M. Kern, and A. N. Nikitin, 2005, Directional dependence of P- and S-wave propagation and polarization in foliated rocks from the Kola superdeep well: Evidence from laboratory measurements and calculations based on TOF neutron diffraction: Tectonophysics, **407**, 25–42, doi: 10.1016/j.tecto.2005.05.029.

Kern, H., T. I. Ivankina, A. N. Nikitin, T. Lokajícek, and Z. Pros, 2008, The effect of oriented microcracks and crystallographic and shape preferred orientation on bulk elastic anisotropy of a foliated biotite gneiss from Outokumpu: Tectonophysics, **457**, 143–149, doi: 10.1016/j.tecto.2008.06.015.

Kocks, U. F., C. N. Tomé, and H. R. Wenk, 2010, Texture and anisotropy — Preferred orientations in polycrystals and their effect on materials properties: Cambridge University Press.

Kröner, E., 1958, Berechnung der elastischen Konstanten des Vielkristalls aus den Konstanten des Einkristalls: Zeitschrift für Physik, **151**, 504–518.

Lebensohn, R. A., 2001, *N*-site modelling of a 3D viscoplastic polycrystal using fast Fourier transform: Acta Materialia, **49**, 2723–2737, doi: 10.1016/S1359-6454(01)00172-0.

Lebensohn, R. A., R. Brenner, O. Castelnau, and A. D. Rollett, 2008, Orientation image-based micromechanical modelling of subgrain texture evolution in polycrystalline copper: Acta Materialia, **56**, 3914–3926, doi: 10.1016/j.actamat.2008.04.016.

Lebensohn, R. A., A. K. Kanjarla, and P. Eisenlohr, 2012, An elasto-viscoplastic formulation based on fast Fourier transforms for the prediction of micromechanical fields in polycrystalline materials: International Journal of Plasticity, **32–33**, 59–69, doi: 10.1016/j.ijplas.2011.12.005.

Lebensohn, R. A., and C. N. Tomé, 1993, A self-consistent anisotropic approach for the simulation of plastic deformation and texture development of polycrystals — Application to zirconium alloys: Acta Metallurgica et Materialia, **41**, 2611–2624, doi: 10.1016/0956-7151(93)90130-K.

Matthies, S., 2010, On the combination of self-consistent and geometric mean elements for the calculation of the elastic properties of textured multi-phase samples: Solid State Phenomena, **160**, 87–93, doi: 10.4028/www.scientific.net/SSP.160.87.

Matthies, S., 2012, GEO-MIX-SELF calculations of the elastic properties of a textured graphite sample at different hydrostatic pressures: Journal of Applied Crystallography, **45**, 1–16, doi: 10.1107/S002188981104338X.

Matthies, S., G. W. Vinel, and K. Helming, 1987, Standard distributions in texture analysis: Akademie-Verlag.

Matthies, S., H.-R. Wenk, and G. W. Vinel, 1988, Some basic concepts of texture analysis and comparison of three methods to calculate orientation distributions from pole figures: Journal of Applied Crystallography, **21**, 285–304, doi: 10.1107/S0021889888000275.

Militzer, B., H.-R. Wenk, S. Stackhouse, and L. Stixrude, 2011, First-principles calculation of the elastic moduli of sheet silicates and their application to shale anisotropy: American Mineralogist, **96**, 125–137, doi: 10.2138/am.2011.3558.

Morris, P. R., 1970, Elastic constants of polycrystals: International Journal of Engineering Science, **8**, 49–61, doi: 10.1016/0020-7225(70)90014-5.

Moulinec, H., and P. Suquet, 1998, Numerical method for computing the overall response of nonlinear composites with complex microstructure: Computational Methods in Applied Mechanics and Engineering, **157**, 69–94.

Nye, J. F., 1957, The physical properties of crystals: Their representation by tensors and matrices: Oxford University Press.

Reuss, A., 1929, Berechnung der Fließgrenze von Mischkristallen auf Grund der Plastizitätsbedingung für Einkristalle: Zeitschrift für Angewandte Mathematik und Mechanik, **9**, 49–58.

Vasin, R. N., H.-R. Wenk, W. Kanitpanyacharoen, S. Matthies, and R. Wirth, 2013, Anisotropy of Kimmeridge shale: Journal of Geophysical Research, Solid Earth, **118**, 1–26, doi: 10.1029/2012JD018174.

Vaughan, M. T., and S. Guggenheim, 1986, Elasticity of muscovite and its relationship to crystal structure: Journal of Geophysical Research, **91**, 4657–4664, doi: 10.1029/JB091iB05p04657.

Voigt, W., 1887, Theoretische Studien über die Elasticitätsverhältnisse der Krystalle: Dieterichsche Verlags.

Wang, Q., L. Burlini, D. Mainprice, and Z. Xu, 2009, Geochemistry, petrofabrics and seismic properties of eclogites from the Chinese Continental Scientific Drilling boreholes in the Sulu UHP terrane, eastern China: Tectonophysics, **475**, 251–266, doi: 10.1016/j.tecto.2008.09.027.

Wenk, H.-R., W. Kanitpanyacharoen, and M. Voltolini, 2010, Preferred orientation of phyllosilicates: Comparison of fault gouge, shale and schist: Journal of Structural Geology, **32**, 478–489, doi: 10.1016/j.jsg.2010.02.003.

Wenk, H.-R., R. N. Vasin, H. Kern, S. Matthies, S. C. Vogel, and T. I. Ivankina, 2012, Revisiting elastic anisotropy of biotite gneiss from the Outokumpu scientific drill hole based on new texture measurements and texture-based velocity calculations: Tectonophysics, **570–571**, 123–134, doi: 10.1016/j.tecto.2012.06.023.

Wenk, H.-R., M. Voltolini, H. Kern, T. Popp, and M. Mazurek, 2008, Anisotropy in shale from Mont Terri: The Leading Edge, **27**, 742–748, doi: 10.1190/1.2944159.